Circularly Polarized Spherical Illumination Reflectometry

Abhijeet Ghosh Tongbo Chen* Pieter Peers† Cyrus A. Wilson Paul Debevec

USC Institute for Creative Technologies

Figure 1: *Renderings under environmental illumination of subjects with spatially varying reflectance acquired using circularly polarized spherical illumination.*

Abstract

We present a novel method for surface reflectometry from a few observations of a scene under a single uniform spherical field of circularly polarized illumination. The method is based on a novel analysis of the Stokes reflectance field of circularly polarized spherical illumination and yields per-pixel estimates of diffuse albedo, specular albedo, index of refraction, and specular roughness of isotropic BRDFs. To infer these reflectance parameters, we measure the Stokes parameters of the reflected light at each pixel by taking four photographs of the scene, consisting of three photographs with differently oriented linear polarizers in front of the camera, and one additional photograph with a circular polarizer. The method only assumes knowledge of surface orientation, for which we make a few additional photometric measurements. We verify our method with three different lighting setups, ranging from specialized to off-the-shelf hardware, which project either discrete or continuous fields of spherical illumination. Our technique offers several benefits: it estimates a more detailed model of per-pixel surface reflectance parameters than previous work, it requires a relatively small number of measurements, it is applicable to a wide range of material types, and it is completely viewpoint independent.

Keywords: Surface reflectometry, circular polarization, Stokes parameters, index of refraction.

*currently at the Munsell Color Science Laboratory, Rochester Institute of Technology.

†currently at The College of William & Mary.

ACM Reference Format
Ghosh, A., Chen, T., Peers, P., Wilson, C., Debevec, P. 2010. Circularly Polarized Spherical Illumination Reflectometry. *ACM Trans. Graph. 29*, 6, Article 162 (December 2010), 11 pages.
DOI = 10.1145/1866158.1866163 http://doi.acm.org/10.1145/1866158.1866163.

1 Introduction

Digitally reproducing the appearance of physical objects such as cultural artifacts, consumer products, material samples, and human faces is a long-standing goal of computer graphics. A variety of techniques for appearance reproduction require photographs of the subject under a subset of the possible illumination conditions and fitting of surface reflectance models to the data to predict the subject's appearance under arbitrary illumination. An ideal process would accurately model the subject's reflectance with just a few photographs. However, in practice, significant compromises are typically made between the accuracy of the reflectance model and the amount of data which must be acquired.

This paper describes a novel data-driven surface reflectometry technique which is able to measure, per visible surface point, diffuse and specular albedo, specular roughness of isotropic BRDFs, and index of refraction. To date, no single acquisition technique captures *all* of these reflectance properties as they vary across the surface of an object. Consequently, some of these characteristics are often omitted or a default value is assumed (for example, the index of refraction). Unlike prior work which infers reflectance information from angularly modulated illumination intensity alone, we measure the complete polarization state of the reflected light under a fixed lighting condition to estimate reflectance parameters.

Specifically, we observe a scene under circularly polarized spherical illumination, and capture four photographs through different polarizing filters in front of the camera to measure the Stokes parameters of the reflected light at each pixel. The combination of a full description of the Stokes parameters and circularly polarized spherical illumination provides a richer description of the reflectance characteristics of the subject. Remarkably, the estimation of diffuse/specular albedo, index of refraction, and specular roughness (assuming known surface orientation), is viewpoint-independent, and only relies on Stokes parameters captured under a *single* uniform full-on spherical illumination condition (4 photographs total). For objects of unknown shape, we can obtain surface orientation from a few (up to 12) additional photometric measurements.

We demonstrate the practicality and robustness of our reflectance acquisition technique and its variants using both continuous and discrete incident illumination setups.

The principal contributions of this work are:

- A novel analysis of circularly polarized illumination based on Mueller calculus applied to reflectance modeling.
- A practical view-independent method for inferring a more complete set of reflectance properties from just a single full-on circularly polarized spherical lighting condition.
- The first method for estimating spatially varying index of refraction of physical subjects.
- The introduction of the concept of a Stokes reflectance field: a construct used to investigate the effects of specular roughness on the Stokes parameters. This tool enables a novel inverse rendering method for inferring spatially varying specular roughness of isotropic BRDFs.

2 Related Work

We discuss related work in two parts: general reflectance measurement and model fitting, and polarization-based reflectance measurement techniques which relate to *polarimetry* and *ellipsometry*.

2.1 Reflectance Measurement and Model Fitting

Describing how an object transforms incident illumination into reflected light is key to reproducing its appearance in computer graphics. For non-translucent materials, the reflectance properties of a surface point are typically described by the the Bidirectional Reflectance Distribution Function (BRDF) [Nicodemus et al. 1977], a 4D function that describes the distribution of reflected light for any incident ray direction. The BRDF of a surface can be exhaustively measured and tabulated in a data-driven way (e.g., [Matusik et al. 2003]), or the measurements can be used to fit an analytic reflectance model (e.g., as in [Marschner et al. 1999]). A large number of analytical BRDFs have been developed, emphasizing various properties such as physical accuracy [Torrance and Sparrow 1967; He et al. 1991], ease of visualization [Ashikhmin et al. 2000], or ease of measurement and fitting of parameters [Lafortune et al. 1997; Ward 1992].

To avoid exhaustive measurement, recent work has focused on obtaining accurate BRDF parameters from fewer measurements. One strategy is to share and/or segment reflectance properties spatially over an object [Georghiades 2003; Goldman et al. 2005; Lensch et al. 2001; Lensch et al. 2003; Zickler et al. 2006], or to illuminate the object with extended light sources [Nayar et al. 1990; Gardner et al. 2003; Ma et al. 2007] instead of point lights.

Our work is most closely related to that of Ghosh et al. [2009] who employ first and second order gradient illumination patterns to infer reflectance parameters (diffuse/specular albedo and specular roughness) for each surface point. While they are able to obtain per-surface point reflectance properties from very few measurements, their method is limited to a single viewpoint because it relies on linearly polarized incident illumination that is carefully tuned to allow for diffuse-specular separation for a specific viewpoint. In contrast, the presented method is also able to estimate reflectance properties per-surface point, but instead of using linear polarization of the incident light field, we employ circularly polarized incident illumination which is defined independent of viewpoint. In addition, the proposed method captures a more complete set of reflectance properties, including index of refraction, and achieves a better signal-to-noise ratio.

2.2 Polarization-Based Reflectance Measurement

In physics, the classic techniques of *polarimetry* and *ellipsometry* are used to characterize properties of electromagnetic waves and thin films. In computer graphics and computer vision, there is also a rich history of measuring polarization to characterize the reflectance properties of physical objects. We can roughly subdivide these into four categories: component separation, material classification, normal estimation, and index of refraction estimation.

Reflectance Component Separation. Separating the diffuse and specular components of surface reflectance is an important component of many appearance acquisition techniques. Most existing separation strategies are either based on color-space heuristics (e.g., [Shafer 1985; Lee et al. 2006; Mallick et al. 2006]), on the polarization-preserving properties of specular reflections [Wolff and Boult 1991; Müller 1996; Debevec et al. 2000; Ma et al. 2007], or a combination of both [Nayar et al. 1993; Nayar et al. 1997; Umeyama and Godin 2004].

Color-space methods are view-independent but often focus on *specular highlight removal*. In order to model specular reflectance characteristics across a surface, accurate separation of both components is needed. Polarization-based methods can be classified based on whether they utilize passive, unpolarized illumination (e.g., [Wolff and Boult 1991; Müller 1996]) or active, polarized illumination (e.g., [Cula et al. 2007; Ma et al. 2007]). Passive methods can suffer from low SNR when there is a significant diffuse reflectance component. Active methods, in general, are either view dependent or require a large number of measurements. Most prior work on polarization-based separation uses linear polarization, although Ma et al. [2007] partially explored the use of circular polarization. In this work, we will further explore the properties of spherical circularly polarized active illumination in order to obtain a view-independent separation of equal quality for every surface orientation, as opposed to Ma et al. whose circular polarization separation technique degrades significantly with increasing angle from normal incidence.

Material Classification. Selecting an appropriate reflectance model depends to a large extent on the underlying material type. The ability to discern dielectric from metallic specular materials can greatly facilitate the choice of an appropriate model. Color-based material classification methods (e.g., [Healey 1992]) can fail in some situations such as when observing a white object under uniform white illumination. Conversely, different polarization-based methods have been developed to discriminate dielectric and metallic materials by exploiting properties such as the Fresnel ratio [Wolff 1990; Wolff and Boult 1991], the polarization phase [Chen and Wolff 1998], or polarization distributions around highlights [Tominaga and Yamamoto 2008].

Normal Estimation. Polarimetry has been used extensively in computer vision for estimating surface normals. A majority of these methods employ passive unpolarized illumination, taking a series of photographs while rotating a linear polarizer in front of the camera. Key to determining the surface orientation per surface point is that the *angle of polarization* determines the direction perpendicular to the plane of incidence, independent of the index of refraction or surface roughness. There are two main strategies to determine the angle within the plane of incidence. A first class employs multiple polarized cameras [Wolff 1989; Wolff and Boult 1991; Rahmann and Canterakis 2001; Miyazaki et al. 2004; Atkinson and Hancock 2005; Sadjadiz and Sadjadi 2007]. However, in this case surface correspondences are required, which can be difficult to accurately obtain. The second class infers surface orientation from the *degree of polarization* and inverting the Fresnel equations. However, the degree of polarization reaches an extremum at the Brewster angle, and thus does not uniquely determine the surface normal. Most prior work focuses on solving this ambiguity [Thilak et al. 2007; Atkinson and Hancock 2007; Atkinson and Hancock 2008; Saito et al. 1999; Miyazaki and Ikeuchi 2007; Miyazaki et al. 2003]. All of these methods require exact knowledge of the index of refraction,

and assume (either implicitly or explicitly) an optically smooth surface (e.g., glass).

The majority of the methods above assume that the incident illumination is unpolarized, and employ a rotating linear polarizer in front of the camera. A notable exception is the method by Koshikawa [1992] who uses right circularly polarized illumination from a point light source to determine surface orientation. However, they ignore the effects of surface roughness and assume a known index of refraction.

Our work follows a different approach. We observe that polarimetry can either provide information on the surface normal assuming a known index of refraction and surface roughness, or vice versa. We note that surface orientation can be robustly estimated from photometric cues, while index of refraction and specular roughness are much more difficult to measure. We therefore employ a photometric method for estimating surface normals, and utilize polarimetry to estimate the remaining reflectance properties.

Index of Refraction. While index of refraction plays an important role in the visual appearance of physical objects, little work in computer graphics has addressed the measurement of the index of refraction of physical objects. One difficulty is that the measurement techniques employed in physics are not readily adaptable to appearance acquisition of objects with spatially varying material properties and free-form shape. Prior work in polarimetry often assumes a known index of refraction, with the exception of [Sadjadiz and Sadjadi 2007] who assume an optically smooth surface, and [Thilak et al. 2007] who employ a polarization-based microfacet BRDF model [Priest and Germer 2000]. Recent work of Dana et al. [2009] measures spatially varying index of refraction of transparent objects using translation of a bidirectional imaging setup over each surface point and detection of the Brewster angle. As noted before, we employ a different strategy. We estimate index of refraction and specular roughness robustly from polarization, obtaining surface orientation from a photometric method. Our method can be used with any reflectance model that includes Fresnel gain.

3 Overview

In this work we propose a novel method for inferring reflectance properties from observations of the four Stokes parameters of an object under circularly polarized incident illumination. We start our exposition with a brief review of the necessary background on polarization and Mueller calculus in Section 4. Using this background, we then derive formulae for inferring reflectance properties (Section 5), assuming known surface orientation, from the four Stokes parameters of each surface point under circularly polarized uniform spherical illumination.

To infer the reflectance properties, we propose a three step procedure. First, the specular and diffuse albedo components are separated by computing the degree of polarization from the Stokes parameters (Section 5.1). Next, index of refraction is estimated from the observed ratio of circularly polarized specular reflections (Section 5.2). Finally, given the index of refraction, an inverse rendering approach is taken to estimate specular roughness (Section 5.3) by matching simulated Stokes parameters with the observed Stokes parameters under circularly polarized uniform spherical illumination.

The above assumes that observations of the Stokes parameters and the surface orientation are available for each surface point. We discuss three different setups and the necessary calibration for measuring these Stokes parameters in Section 6. Additionally, we employ and extend the method of Ma et al. [2007] to capture surface orientation independently of viewpoint (i.e., the illumination and polarization conditions are invariant to changes in viewpoint).

4 Polarization and Mueller Calculus

Before detailing the proposed polarization-based appearance measurement method in the next section, we will first review the relevant background on polarization and Mueller calculus. Since our final goal is to infer surface reflectance, we limit this discussion to reflection only, and omit transmission. We refer the interested reader to [Collett 2005] for a more in depth overview of polarization and Mueller calculus.

Polarization describes the mutually perpendicular components of the transverse oscillation of light waves. According to Mueller calculus, the polarization state of light can be described by the 4-element Stokes vector: $\mathbf{s} = (s_0, s_1, s_2, s_3)$, where: s_0 represents the total power or intensity, s_1 the power of 0° linear polarization (horizontal), s_2 the power of $+45^\circ$ linear polarization, and s_3 the power of right circular polarization. During light transport, a Stokes vector $\mathbf{s}$ is transformed to a new Stokes vector, when a polarized ray interacts with a surface. This transformation can be exactly described by linear operators in Mueller calculus as:

$$\mathbf{s}' = \mathbf{C}(\phi)\mathbf{D}(\delta;\mathbf{n})\mathbf{R}(\theta;\mathbf{n})\mathbf{C}(-\phi)\mathbf{s}. \tag{1}$$

$\mathbf{C}$ is the Mueller rotation matrix for a given ray and is defined as:

$$\mathbf{C} = \begin{pmatrix} 1 & 0 & 0 & 0 \\ 0 & \cos 2\phi & -\sin 2\phi & 0 \\ 0 & \sin 2\phi & \cos 2\phi & 0 \\ 0 & 0 & 0 & 1 \end{pmatrix}, \tag{2}$$

where ϕ is the angle between the plane of incidence and the x-axis in the observation coordinate system. The plane of incidence is the plane containing the incident ray, the exitant ray, and the surface normal $\mathbf{n}$.

$\mathbf{R}$ is the Mueller reflection matrix, which models the actual surface reflection, and is defined as:

$$\mathbf{R} = \begin{pmatrix} \frac{\mathbf{R}_\parallel + \mathbf{R}_\perp}{2} & \frac{\mathbf{R}_\parallel - \mathbf{R}_\perp}{2} & 0 & 0 \\ \frac{\mathbf{R}_\parallel - \mathbf{R}_\perp}{2} & \frac{\mathbf{R}_\parallel + \mathbf{R}_\perp}{2} & 0 & 0 \\ 0 & 0 & \sqrt{\mathbf{R}_\parallel \mathbf{R}_\perp} & 0 \\ 0 & 0 & 0 & \sqrt{\mathbf{R}_\parallel \mathbf{R}_\perp} \end{pmatrix}, \tag{3}$$

where $\mathbf{R}_\parallel$ and $\mathbf{R}_\perp$ are the Fresnel equations for the parallel and perpendicular components, respectively, as functions of the incident angle θ.

Finally, $\mathbf{D}$ represents the retardation Mueller matrix:

$$\mathbf{D} = \begin{pmatrix} 1 & 0 & 0 & 0 \\ 0 & 1 & 0 & 0 \\ 0 & 0 & \cos\delta & \sin\delta \\ 0 & 0 & -\sin\delta & \cos\delta \end{pmatrix}, \tag{4}$$

and δ is the phase shift. This phase shift differs depending on whether the material is a dielectric or a metal. For dielectric materials it is either 180° when $\theta \leq \theta_B$, or 0° when $\theta > \theta_B$, with the Brewster angle θ_B, which is related to the index of refraction (η) as: $\tan\theta_B = \eta$. For metallic materials, the phase shift decreases continuously with θ, from 180° at $\theta = 0^\circ$, to 0° at $\theta = 180^\circ$. The shape of the falloff depends on both components of the complex index of refraction $\eta + i\kappa$, where the η is the refractive index (comparable to that of dielectrics), and κ the extinction coefficient. We refer to [Chen and Wolff 1998] for a detailed description.

The linear transform of Equation 1 holds for pure specular reflections only. However, the polarization state for rough specular reflections can still be modeled in this manner with a micro-facet BRDF model. Each micro-facet transforms the Stokes vector according to Mueller calculus. Due to the linearity of light (and thus the Stokes

vectors), the aggregate Stokes vector after rough specular reflection can be computed as:

$$\mathbf{s}''(\omega_o) = \int_\Omega \mathbf{f}(\mathbf{n}; m; \omega_i, \omega_o)\mathbf{s}'(\omega_i)d\omega_i, \tag{5}$$

where $\mathbf{f}$ defines the micro-facet BRDF model (times foreshortening) with roughness m over incident and exitant directions ω_i and ω_o respectively. In this paper we use a Torrance-Sparrow [1967] BRDF to model rough specular reflections.

5 Reflectance from Stokes Observations

Given the above relationships, it follows that the reflected Stokes vector may be used to recover reflectance parameters. Here we show how to infer per-pixel reflectance properties (albedo, index of refraction, and specular roughness) from the observation of the Stokes vector $\mathbf{s}$ under circularly polarized uniform spherical illumination and surface normal $\mathbf{n}$.

5.1 Diffuse/Specular Albedo

In order to compute both diffuse and specular albedo, we need to be able to distinguish which part of the observed radiance underwent a diffuse or specular reflection.

Polarization has previously been used as a cue to distinguish between diffuse and specular reflections [Wolff and Boult 1991; Müller 1996; Cula et al. 2007; Ma et al. 2007]. The key idea is that polarized radiance can only be the result of specular reflection under polarized incident illumination. Diffuse reflections, on the other hand, are the aggregate result of multiple scattering events, and hence depolarize the reflected incident radiance. We can formalize this relation by looking at the degree of polarization. The degree of polarization is defined as the fraction of the observed radiance which is polarized: $DOP = (\sqrt{s_1^2 + s_2^2 + s_3^2})/s_0$. Hence, it is the ratio of specular intensity to total intensity observed under polarized incident illumination. Multiplying both sides of this equation with s_0 yields the absolute amount of observed specularly reflected radiance: $DOP \times s_0$. The diffuse reflected radiance is then defined as: $(1 - DOP) \times s_0$.

This relation holds for any type of polarized incident illumination. In the case of polarized uniform spherical illumination, it effectively becomes an integration of the reflectance, at each surface point, over the hemisphere of incident directions. Thus, the separated diffuse and specular components under uniform spherical illumination correspond directly to the diffuse albedo ρ_d and specular albedo ρ_s, respectively.

5.2 Index of Refraction

Index of refraction is an important and integral component that affects the appearance of physical objects. Prior work often approximates indices of refraction from physical tables based on material type. However, it is not always possible to identify the exact material type of an object. Moreover, this approach ignores spatial variation in index of refraction.

In this section, we propose a novel method for inferring spatially varying indices of refraction from circularly polarized uniform spherical illumination. We first derive the necessary formulae for the estimation of the index of refraction for mirror-like dielectric materials. Next, we investigate the applicability of the derived formulae for mirror-like metallic materials. Finally, we expand this theory to comprise rough specular materials.

Mirror-like Specular Dielectric Materials. Consider the case of reflections of a mirror-like specular dielectric material with no specular roughness. In this case the exact amount of total reflected radiance is governed by the well-known Fresnel equations, which are a function of incident angle θ and the index of refraction η:

$$\mathbf{R}_\perp = \left(\frac{\cos\theta - \eta\sqrt{1 - \left(\frac{1}{\eta}\sin\theta\right)^2}}{\cos\theta + \eta\sqrt{1 - \left(\frac{1}{\eta}\sin\theta\right)^2}} \right)^2, \tag{6}$$

$$\mathbf{R}_\parallel = \left(\frac{\sqrt{1 - \left(\frac{1}{\eta}\sin\theta\right)^2} - \eta\cos\theta}{\sqrt{1 - \left(\frac{1}{\eta}\sin\theta\right)^2} + \eta\cos\theta} \right)^2, \tag{7}$$

From this we can write η as a function of $\mathbf{R}_\parallel$ and $\mathbf{R}_\perp$:

$$\eta^2 = \frac{(1 + \sqrt{\mathbf{R}_\parallel})(1 + \sqrt{\mathbf{R}_\perp})}{(1 - \sqrt{\mathbf{R}_\parallel})(1 - \sqrt{\mathbf{R}_\perp})}. \tag{8}$$

It follows that once we have knowledge of $\mathbf{R}_\perp$ and $\mathbf{R}_\parallel$, η can be easily computed. Note that Equation (8) depends only on $\mathbf{R}_\parallel$ and $\mathbf{R}_\perp$, and has no further dependence on the incident angle θ.

To infer $\mathbf{R}_\perp$ and $\mathbf{R}_\parallel$ from observation under uniform spherical illumination, we consider the following. For a mirror-like material, only a single incident direction contributes to the observed specular radiance for a given surface point. The observed Stokes vector in that case is: $\mathbf{C}(\phi)\mathbf{D}(\delta;\mathbf{n})\mathbf{R}(\theta;\mathbf{n})\mathbf{C}(-\phi)\mathbf{s}$, with $\mathbf{s} = (1,0,0,1)$ for uniform spherical right-circularly-polarized illumination. From Equation (2) we observe that the first and last component of the observed Stokes vector (s_0 and s_3) are not affected by the Mueller rotation matrices $\mathbf{C}(\phi)$ and $\mathbf{C}(-\phi)$. Writing out these two components explicitly yields:

$$s_0 = \frac{1}{2}(\mathbf{R}_\parallel + \mathbf{R}_\perp) + \rho_d, \tag{9}$$

$$s_3 = \pm\sqrt{\mathbf{R}_\parallel \mathbf{R}_\perp}, \tag{10}$$

where the sign flip is due to the retardation matrix (Equation (4)), i.e., a negative sign if $\theta \leq \theta_B$ and a positive sign if $\theta > \theta_B$. Substituting for $\mathbf{R}_\perp$ yields the following equation:

$$s_3 = \pm\sqrt{2\hat{s_0}\mathbf{R}_\parallel - \mathbf{R}_\parallel^2}, \tag{11}$$

where $\hat{s_0} = s_0 - \rho_d$. A similar equation can be obtained by substituting for $\mathbf{R}_\parallel$; hence, squaring both sides and solving the resulting quadratic equation yields two solutions which correspond to $\mathbf{R}_\parallel$ and $\mathbf{R}_\perp$. To determine which solution corresponds to $\mathbf{R}_\parallel$ and which to $\mathbf{R}_\perp$, we use the fundamental property that $\mathbf{R}_\perp \geq \mathbf{R}_\parallel$. Additionally, by squaring both sides, we lose the effect of the sign change around the Brewster angle θ_B. We correct for this by negating each $\sqrt{\mathbf{R}_\parallel}$ in Equation (8) when $\theta > \theta_B$ (inferred from the sign of s_3). Once $\mathbf{R}_\parallel$ and $\mathbf{R}_\perp$ are known, η can be computed using Equation (8).

Mirror-like Specular Metallic Materials. The above derivation only holds for dielectric materials. The index of refraction for metallic materials is a complex number, where the real part η is the refractive index, and the imaginary part κ is the extinction coefficient. However, estimating these parameters from spherical illumination is difficult. Note that using a single point light source also does not solve the problem, since (1) the measurements become view-dependent, and (2) only a small portion of the surface will specularly reflect the incident light toward the camera, making it difficult to estimate the index of refraction for all surface points simultaneously.

Nevertheless, empirically we found that by approximating the complex index of refraction by a single real number (i.e., applying Equation (8) as if it were a dielectric material), we still obtain a

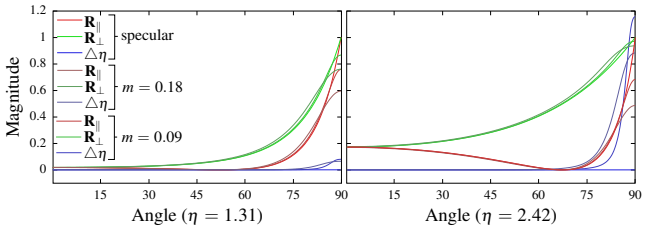

Figure 2: ***Effects of Specular Roughness on Index of Refraction.*** *The L_1 error on the index of refraction is plotted for two indices of refraction and for three specular roughness values for the Torrance-Sparrow BRDF model. Also shown are the approximate Fresnel components $\mathbf{R}_\parallel$ and $\mathbf{R}_\perp$, used to infer the index of refraction, computed from the observed Stokes components s_0 and s_3.*

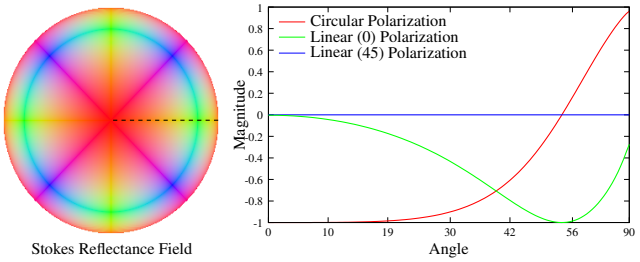

Figure 3: ***Stokes Reflectance Field*** *visualization (**Left**) for a mirror-like BRDF with an index of refraction of 1.38 under full-on circularly polarized illumination. The red, green, and blue color components depict the absolute values of s_3, s_1 and s_2 Stokes parameters, respectively. **Right**: A plot of s_3, s_1 and s_2 for the cross section of the Stokes reflectance field marked by the dashed line.*

good approximation for the unpolarized Fresnel curves commonly used in rendering for near normal incidence.

Rough Specular Materials. The above discussion assumed a mirror-like dielectric material. As noted in Section 4, the effects on the Stokes vector resulting from a rough specular reflection can be modeled using a micro-facet BRDF model. As a result, we observe a convolution of the Stokes vector (a function of θ) with the micro-facet BRDF. Theoretically, this invalidates Equation (8). Nevertheless, we can still compute approximate Fresnel components by applying Equation (11) on the observed s_0 and s_3 under (uniform) spherical illumination.

To better understand the limits of this approximation, we plot the approximate Fresnel components computed from the Stokes components s_0 and s_3 for BRDFs of increasing specular roughness for two plausible different indices of refraction (ice and diamond) in Figure 2. As expected, for nearly mirror-like BRDFs a good approximation for the index of refraction is found over the whole range of incident lighting directions. For rougher specular materials, we still find a good approximation for angles less than the Brewster angle, where the Fresnel components are nearly constant. We found that these observations hold for realistic ranges of the index of refraction of dielectrics. For angles larger than the Brewster angle, we found that for low indices of refraction, a good approximation can still be found. This shows, that under a wide range of conditions, Equation (8) still yields a good approximation to the index of refraction for rough specular surfaces.

5.3 Specular Roughness

Stokes Reflectance Field. To estimate specular roughness parameters, we must first gain better insight into the effect of specular roughness and index of refraction on the observed Stokes vectors. For this we develop the concept of a *Stokes reflectance field*, which is a visualization tool to help assess the influence of different material appearance parameters on the polarization state of the reflected light. A Stokes reflectance field is a description of the Stokes vectors resulting from a single surface interaction, under a user-defined incident light field, computed for every surface normal direction. In this work, we restrict the analysis of the Stokes reflectance field to isotropic BRDFs.

Figure 3 (left) shows an example of such a Stokes reflectance field for a mirror-like BRDF and an index of refraction of 1.38, under uniform full-on (constant from all directions) right circularly polarized incident illumination. For visualization purposes, we have mapped the absolute magnitude of s_3, s_1 and s_2 to the R, G and B color channels, respectively.

In the visualization of the Stokes reflectance field in Figure 3 (left) we can note some interesting properties. First, there are two apparent cross-like structures. These indicate surface normal directions at which s_1 (horizontal linear) and s_2 (45° linear), respectively, are zero. Second, a circular structure is visible around 54°. This is where the magnitude of linear polarization is maximal, i.e., $s_1^2 + s_2^2 = 1$, and the magnitude of circular polarization is zero; it corresponds to the Brewster angle. This can also be clearly seen in the 1D cross-section of the Stokes reflectance field shown in Figure 3 (right).

Effects on Stokes Reflectance Field. We can now use the Stokes reflectance fields of circularly polarized illumination to investigate the relation between surface orientation, index of refraction, and specular roughness.

Figure 4, top row, shows the Stokes reflectance field for increasing indices of refraction under uniform full-on spherical illumination and for a mirror-like material. One can see that as the index of refraction increases, the relative role of linear polarization decreases, and that the Brewster angle, recognizable by the bluish ring where s_3 is zero, is pushed outward. This is further corroborated by the cross section plots of the s_3 component of the Stokes field. Increasing the index of refraction has a sharpening effect on the s_3 curve, pushing circularly polarized power towards larger incident angles.

A similar analysis can be performed to study the impact of specular roughness. Figure 4, bottom row, shows the Stokes field for increasing specular roughness, under uniform spherical illumination and for a fixed index of refraction (1.40). Increasing specular roughness (i.e., making the material less specular) has the effect of increasing the relative impact of linear polarization, and decreasing the overall influence of circular polarization. The Brewster angle moves inward toward normal incidence. The s_3 cross-section plots show a blurring effect with increasing roughness.

Inverse Rendering. The previous analysis showed that the Stokes reflectance field is influenced by both specular roughness as well as index of refraction. In Section 5.2 we showed how the index of refraction can be approximated without knowledge of specular roughness. Combined with knowledge of the surface normal, this should allow one to compute the roughness from the observed Stokes vector. However, the exact relation between the Stokes vector, index of refraction, surface normal, and specular roughness depends on the particular reflectance model used. In order to maintain flexibility in choosing any reflectance model that supports Fresnel curves, we opt for an inverse rendering approach to infer specular roughness.

Given an a-priori reflectance model, estimated index of refraction, surface normal, and a postulated specular roughness value, we can compute the magnitude of circular polarization under uniform spherical illumination using Monte Carlo integration:

$$\tilde{s_3}^m = \int_\Omega \mathbf{f}(\mathbf{n}; m; \theta) \cos\delta \sqrt{\mathbf{R}_\parallel(\eta;\theta)\mathbf{R}_\perp(\eta;\theta)}\, d\omega, \qquad (12)$$

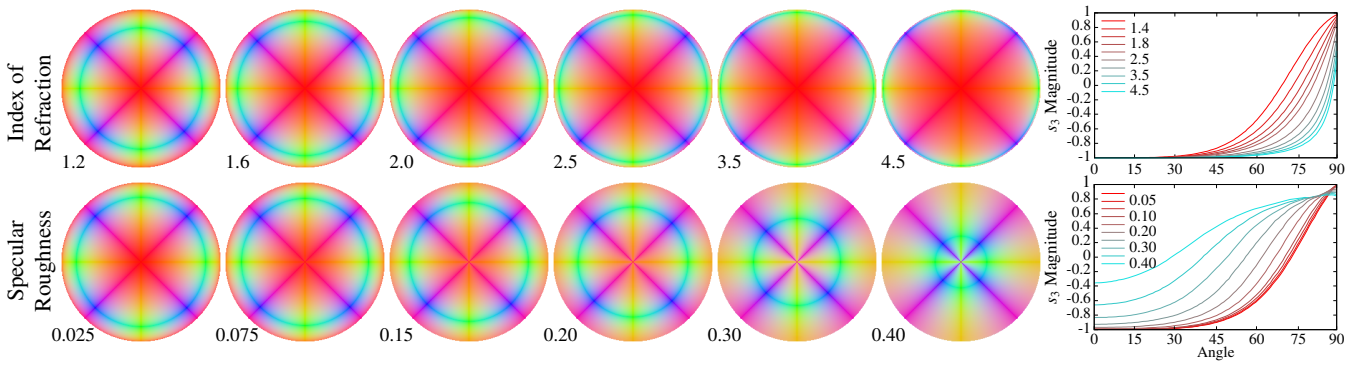

Figure 4: ***Effects of Index of Refraction and Specular Roughness on the Stokes Reflectance Field. Top:*** *varying index of refraction for fixed specular roughness (i.e., mirror-like BRDF). Increasing index of refraction has a sharpening effect on the s_3 component of the Stokes field, and pushes the Brewster angle further back.* ***Bottom:*** *varying specular roughness for a fixed index of refraction ($\eta = 1.40$). Increasing specular roughness flattens the s_3 component of the Stokes reflectance field, and moves the Brewster angle closer to normal incidence.*

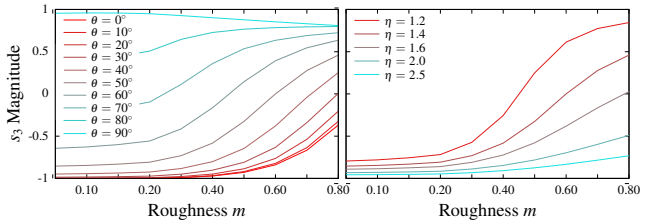

Figure 5: $\tilde{s_3}^m$ ***as a Function of Specular Roughness. Left:*** $\tilde{s_3}^m$ *for selected incident directions and a fixed index of refraction $\eta = 1.40$.* ***Right:*** $\tilde{s_3}^m$ *for selected indices of refraction and a fixed $\theta = 50°$.*

where $\mathbf{f}$ is the a-priori chosen reflectance model (times foreshortening), defined by the surface normal $\mathbf{n}$, the specular roughness m, and incident direction θ. Figure 5 (left) shows $\tilde{s_3}^m$ curves as a function of roughness m for selected incident angles θ, and for a fixed index of refraction $\eta = 1.40$. Figure 5 (right) shows $\tilde{s_3}^m$ for selected values of index of refraction for a fixed incident angle $\theta = 50°$. From this figure we can make the following two observations:

1. the curves $\tilde{s_3}^m$ are monotonic, and are thus easily searched to find the best match to the observed circular component s_3, and
2. the change between different curves is smooth.

Observation (1) implies that we can find a unique solution by matching $\tilde{s_3}^m$ to the observed s_3 component. Observation (2) implies that any error (e.g., due to measurement noise) will still yield a good approximation.

This allows us to formulate the following strategy for estimating the specular roughness. We start by eliminating the specular albedo from the observed circular magnitude by normalizing the fourth Stokes component: $\tilde{s_3} = s_3/\sqrt{s_1^2 + s_2^2 + s_3^2}$. We then find the optimal roughness as: $m = \arg\min_x ||\tilde{s_3}^m - \tilde{s_3}||_2$.

It is possible to precompute all $\tilde{s_3}^m$ curves by exploiting observation (2). Since these curves change smoothly with varying index of refraction and normal, we can create a lookup table $\mathbf{T}(\mathbf{n}, \eta, m)$, which is densely sampled in the first coordinate, and sparsely in the other two. Given an $\mathbf{n}$ and an index of refraction η, we perform a linear interpolation to compute a densely sampled function $\tilde{s_3}^m$, which can then be searched as before.

5.4 Summary

Given the per-pixel observations of the Stokes vectors $\mathbf{s} = (s_0, s_1, s_2, s_3)$ under circularly polarized uniform spherical illumination, and surface orientation $\mathbf{n}$, we compute the per-pixel reflectance properties as follows. We start by computing the diffuse and specular albedo, which are directly related to the degree of polarization. Next, we estimate the index of refraction. For this we first compute the Fresnel components $\mathbf{R}_\parallel$ and $\mathbf{R}_\perp$ from s_3 using Equation (11), and use them in conjunction with Equation (8) to obtain the index of refraction. Finally, the estimated specular albedo and index of refraction are used to optimize for specular roughness that explains the observations of s_3 best.

6 Measurement

The previous exposition assumes that observations of the Stokes parameters and surface normals are available for every visible surface point. In this section we first discuss possible techniques for acquiring Stokes vectors (Section 6.1) and surface normals (Section 6.2). Next, we introduce three different practical setups for generating the necessary incident polarized light fields (Section 6.3).

6.1 Measurement of Stokes Vectors

Direct observation of the Stokes vectors is difficult because typical polarizers do not block unpolarized light completely. In order to minimize the impact of polarizer inefficiency, we compute the Stokes parameters indirectly from four different measurements. Specifically, we capture the scene illuminated by right circularly polarized illumination, and record four photographs with the following polarizers in front of the camera: a linear polarizer rotated $0°$ (P_H), $45°$ (P_{45}), and $90°$ (P_V), and a (left) circular polarizer ($P_\circ$). We can then robustly compute the Stokes vector components as: $s_0 = P_H + P_V$, $s_1 = P_H - P_V$, $s_2 = 2P_{45} - s_0$, and $s_3 = s_0 - 2P_\circ$. Note that each polarized image receives $(50 + \varepsilon)\%$ unpolarized radiance. Thus, with the exception of s_0, this unpolarized radiance is removed by the subtraction. s_0 will overestimate the unpolarized radiance by a factor of 2ε. However, this will only impact the computation of the diffuse albedo.

6.2 Surface Normal Acquisition

The fastest and most convenient way of acquiring surface normals per pixel, for objects with unknown shape, is to employ a photometric stereo technique. While any method can be employed, we opt for a method based on the polarized spherical gradient photometric stereo technique of Ma et al. [2007]: $\tilde{\mathbf{n}} = 2(X_s, Y_s, Z_s) - F_s$, where F_s, X_s, Y_s and Z_s are the specular images of the object under the full-on, X, Y, and Z gradient illumination conditions. Normalizing this vector yields the surface normal: $\mathbf{n} = \frac{\tilde{\mathbf{n}}}{||\tilde{\mathbf{n}}||}$. Ma et al.

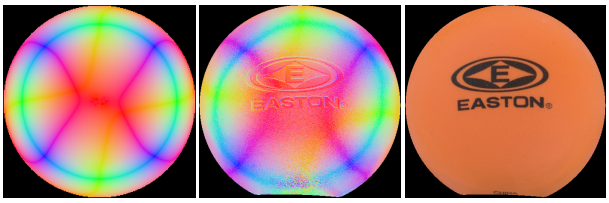

(a) Simulated Stokes (b) Measured Stokes (c) Spherical object

Figure 6: ***Measured Stokes field*** *with off-the-shelf circular polarizers exhibiting slight ellipticity. (a) Simulated Stokes field with measured ellipticity. (b) Measured Stokes field. (c) Measured spherical object - a rubber ball.*

employ linear polarization to compute the specular images of the scene under each lighting condition. The disadvantage of this approach is that it is restricted to single viewpoint capture because the linear polarization incident light field needs to be tuned for a particular viewpoint. Instead of using linear polarization, we employ circularly polarized incident light fields, and employ the diffuse-specular separation method discussed in Section 5.1. This allows us to compute surface normals for any viewpoint without making any changes to the incident lighting or polarization field. Note that the X, Y, and Z lighting conditions are defined in world space (aligned with the emitter), and not in the frame of the camera. However, a simple rotation is sufficient to transform the world-space normals to camera-space normals.

6.3 Setup

We propose three different setups for generating the required lighting conditions. We will first briefly describe these setups, followed by a comparison of the advantages and disadvantages of each setup.

LED Sphere. The first setup consists of an LED sphere with approximately 150 individually controllable LED lights, each covered with a right circular polarizer. The subject is supported at the center of the sphere and observed by a camera placed at any position outside the sphere. In front of the camera we mount a motorized filter wheel containing three differently oriented linear polarizers (45° difference), and one left circular polarizer. For each filter, we take a cycle of four photographs, and between each photograph we change the lighting emitted by the sphere (i.e., 3 gradient lighting condition and a full-on uniform lighting condition). After each cycle of four lighting conditions, we rotate the wheel such that the next filter covers the lens.

Ideally, the right circular polarizers covering the LED lights should filter out any unpolarized and linear polarized illumination. Unfortunately, the efficiency of off-the-shelf polarizers is not perfect. Consequently, besides unpolarized light, there is also some linear polarized light (both 0° and 45°) leaking through, resulting in a slightly elliptically polarized light field. We measured the Stokes parameters of one LED light to be $(1, 0.09, 0.097, 0.96)$ averaged over several random orientations of the right circular polarizer. Even though the power of the linear Stokes parameters is minute, its effect on the Stokes reflectance field is measurable and needs to be accounted for. As can be seen in Figure 6, the purple and yellow lines representing 0° and 45° linear polarization in the Stokes reflectance field no longer meet at the center but diverge slightly. Fortunately, both linear components are of approximately the same magnitude, making it roughly independent on the exact placement of the LED on the dome, allowing us to compensate for this effect by using the same measured Stokes vector for every incident lighting direction during inverse rendering.

Reflective Dome. Our second setup features a hemispherical dome of the form described in [Peers et al. 2006]. The inside of the dome is coated with a rough specular paint which maintains polarization. The object is placed near the center of the hemisphere, and is indirectly illuminated (reflected from the dome) by a projector equipped with a fish-eye lens. The camera observes the object through a hole at the apex of the dome, equipped with a polarization wheel as before. To polarize the the incident light field, a right circular polarizer is placed between the lens and the DLP chip of the projector. Due to the complex light interactions, the incident light field is slightly elliptically polarized. We perform both radiometric and geometric calibration. For radiometric calibration, we measure the gamma curve of the projector, and inversely apply it to the illumination patterns. We then capture a mirrored sphere under the four gradient conditions. We create a mapping between the normalized observed X, Y and Z gradient pixels and the target normal directions computed by overlaying the mirrored sphere with a virtual sphere of identical radius. To accurately calibrate the incident Stokes field, we also capture a high gloss black plastic sphere under uniform illumination, and compute the Stokes reflectance field. We then inversely apply Equation 1 on the observations to obtain the incident Stokes field.

Description	η from s_0 and s_3	η from θ_B	Relative Error	Std. Dev.
Toy baseball	1.247	1.263	1.2%	0.045
Rubber ball	1.403	1.381	1.5%	0.034
Gell stress ball	1.502	1.507	0.3%	0.031
Christmas Ornament	2.12	2.15	1.3%	0.029

Table 1: ***Index of Refraction Validation.*** *For a set of homogeneous spherical objects, we compare the average (and standard deviation) index of refraction obtained with the proposed method with that obtained by measuring the Brewster angle θ_B.*

Polarized CRT. The final setup consists of a CRT screen with a right circular polarization sheet in front. Radiometric and geometric calibration are performed similarly to the reflective dome setup.

Comparison. Each of the setups has strengths and weaknesses. The LED sphere has the advantage that it covers the whole sphere of incident lighting directions, but at a low sampling rate: just 150 directions. This places a limit on the specular roughness of the materials that can be captured; very mirror-like materials will be measured with less accuracy. The reflective dome, on the other hand, covers less of the sphere of incident lighting directions (approximately half), but with a near-continuous illumination field of approximately 1M lighting directions. The partial coverage of the sphere of incident direction effectively places a limit on range of surface normals that can be captured. Finally, the polarized CRT screen has the advantage that it is inexpensive to create, and has a very high sampling rate. However, it only covers a very small portion of the sphere of incident lighting directions, and thus is only suitable for nearly flat samples.

7 Results and Discussion

Validation and Comparison. To validate the accuracy of the index of refraction estimation, we capture and compute the Stokes reflectance field of a homogeneous spherical object using the LED sphere, and detect the Brewster angle (i.e., the zero crossing of s_3). From this measurement of Brewster angle we can compute the index of refraction by: $\tan\theta_B = \eta$. We compare this independently computed index of refraction to the average index of refraction estimated using the method described in section 5.2. Table 1 shows the results. As shown by the relative error, the estimated indices of refraction are a close match.

To validate the accuracy of the specular roughness estimation, we compare the specular roughness obtained using the proposed

Description	m from Stokes	m from point source	Relative Error	Std. Dev.
Gell stress ball	0.166	0.162	2.4%	0.037
Rubber ball	0.191	0.187	2.1%	0.035
Ping-pong ball	0.214	0.212	0.9%	0.043
Wooden ball	0.314	0.312	0.6%	0.048

Table 2: ***Specular Roughness Validation.*** *We compare the average specular roughness (and standard deviation) obtained with our method on homogeneous spherical objects with the specular roughness fit obtained by measuring the specular lobe using a frontal point-lighting condition.*

Figure 7: ***Homogeneous spherical objects*** *of varying specular roughness illuminated by a frontal point light source. Left to right: red gell stress ball, orange rubber ball, green-yellow toy baseball, wooden ball.*

(a) Stokes (b) Second order gradients

Figure 8: ***Comparison of estimated per pixel specular roughness*** *with the technique of Ghosh et al. [2009].* ***(a)*** *Specular roughness estimated from the Stokes measurements of constant full-on illumination.* ***(b)*** *Specular roughness from polarization difference imaging of second order spherical gradients.*

method (using the LED sphere) on homogeneous spherical objects with specular roughness fitted to the specular lobe observed when illuminating the object with frontal point-lighting (Figure 7). The results are listed in Table 2. Overall, the obtained specular roughness is a close match to the reference solution.

We also compare our estimates of specular roughness from Stokes parameters to estimates obtained using the second order gradient method of Ghosh et al. [2009] for a Christmas tree ornament with a set of snowmen with spatially varying reflectance acquired in the reflective dome setup (Figure 8). Following are the pairwise (Stokes versus second-order) average specular roughness estimates (m) for various regions on the snowmen: hats ($0.088/0.108$), scarves ($0.1/0.098$), body ($0.255/0.238$), wooden base ($0.107, 0.072$). As can be seen, the relative difference in the average region-wise estimates obtained by the two techniques is not large. However, we note that the specular roughness obtained from Stokes parameters of the constant full-on illumination is much less dependent on local surface orientation than estimates made with second order spherical gradients, greatly improving the robustness of the estimates.

Results. To further demonstrate the technique we captured several scenes comprising a wide range of material types using the setups discussed in the previous section. Figure 11 shows the different reflectance components obtained using the proposed method. The top two subjects were each acquired with 16 measurements using the LED sphere (a full-on plus three additional gradient lighting conditions for surface normal estimation, each with 4 different polarizers in front of the camera). The material properties measured for the face (top row) are sufficient to produce photoreal renderings under lighting conditions vastly different than those under which

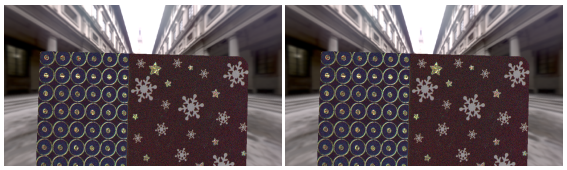

(a) Full-on illumination (b) Gradient illumination

Figure 9: ***Comparison of estimated reflectance properties*** *of a spatially varying flat sample from just the four Stokes measurements under constant full-on illumination* ***(a)*** *with that obtained with surface normals measured with spherical gradients* ***(b)****.*

the subject was captured, such as a point light (e), or environment illumination (Figure 1 and video). The same technique and measurement device works equally well for a significantly different material: the painted wood wall hanging (second row). The third object, a Christmas tree ornament with five snowmen, was captured with only 10 measurements each, using the rough specular dome setup. We reduced the number of measurements to 10 for the rough specular dome setup by only capturing two polarization states (left- and right-circularly polarized) for the gradient illumination images used for normal estimation. In this case we performed diffuse-specular separation of the gradient illumination images using simple polarization differencing. Usually, this reduces the quality of the surface normal estimation for normal directions at larger angles to the viewing direction. However, in this setup, surface normal estimation is already limited to no more than a 45° cone around the view direction, since the rough specular dome only covers the frontal hemisphere. Finally, the bottom row presents results of a spatially-varying flat sample, obtained using a circularly polarized CRT illumination device.

The two right columns of Figure 11 show a rendering of each scene under point light source illumination compared to a reference photograph. In all cases, the observable diffuse and specular components of the reflectance match well qualitatively, but differences are noticeable. For results obtained with the LED sphere, we observe that reproduced specular highlights differ from the reference photographs on very mirror-like surfaces. This is expected given the limited discretized lighting resolution of the LED sphere. For results captured using the rough specular hemisphere, we see poor surface normal estimation quality for normals pointing away from the camera, resulting in noisy estimates for these surface points. This is also expected due to the limited angular coverage of the hemisphere. Figure 1 shows some of the acquired subjects rendered as lit by complex natural illumination. The supplementary video contains additional results rendered with animated natural illumination to better show the spatial coherence of the estimated reflectance.

One advantage of the proposed technique is that for objects of known surface shape (e.g., a flat sample), the measurement of the four Stokes parameters under *only* constant full-on circularly polarized illumination is sufficient to estimate spatially varying surface reflectance parameters. This makes this setup an ideal low cost solution for measuring SVBRDFs from planar samples. Figure 9 demonstrates this for a spatially varying flat sample with minor surface variation, illuminated by a polarized CRT screen. The reflectance parameters estimated from just four Stokes measurements (left) produce identical renderings to those obtained with the extended set of ten measurements (right).

As a final result, we investigate the impact of using a fixed index of refraction versus using spatially varying indices of refraction. We illustrate this in Figure 10. Here we computed the *optimal* specular roughness for the constant index of refraction case. As expected the differences are subtle, but noticeable. For example, the speckle on the glitter at the bottom is not faithfully reproduced when employ-

(a) Spatially varying IOR (b) Constant IOR

Figure 10: ***Comparison of per pixel index of refraction*** *on the estimated specular roughness (top row) and renderings in the Grace cathedral environment (bottom row).* ***(a)*** *Spatially varying index of refraction obtained from the Stokes measurements.* ***(b)*** *Constant index of refraction ($\eta = 1.4$) across the surface.*

ing a constant index of refraction. In general, specular highlights appear duller (e.g., on the hats, the brown sled, and the metallic hooks) as the specular roughness is overestimated when assuming a constant index of refraction.

Discussion and Limitations. The estimated index of refraction corresponds exactly to the physical index of refraction only for perfectly specular, purely dielectric materials. For more general dielectrics and composites, the index of refraction estimated by this approach deviates from the true index of refraction of the material. However, this approximate index of refraction is still accurate enough to plausibly reproduce the unpolarized reflectance behavior of such objects for photorealistic renderings. For metallic materials, the real approximation of the complex index of refraction approximates the reflectance behavior well if estimated from observations near normal incidence, and for metals with low κ or high η. In future work, we would like to investigate methods to estimate the actual complex index of refraction for metals in general.

The quality of the estimated specular roughness parameters depends significantly on the accuracy of the estimated surface normals. This limitation is shared by most existing roughness estimation methods. For very mirror-like materials, the quality of the roughness estimate is further limited with regard to precision: for low levels of specular roughness, differences in specular roughness produce only small changes in observed s_3, as shown in Figure 5. Factors such as camera noise and even small errors in normal estimation can therefore have a significant impact on the roughness estimated for such materials. Given that we rely on the shape of the s_3 curve for estimating specular roughness, less reliable estimates are obtained around the Brewster angle. Finally, occlusions and inter-reflections can also add bias to the estimate of reflectance properties for materials exhibiting a broad specular lobe.

Circular versus Linear. We employ circular polarization in this work in conjunction with measurements of Stokes parameters in order to infer surface reflectance parameters. In this context, circular polarization has certain advantages over linear polarization:

- A circularly polarized incident light field enables viewpoint independent measurements of reflectance fields. Linearly polarized incident illumination, on the other hand, becomes viewpoint dependent after reflection (requiring, for example, viewpoint-specific tuning of the linear polarization field as in Ma et al. 2007). Hence employing circularly polarized illumination allows us to create more general measurement setups such as the reflective dome setup.
- The usage of circular polarization makes it possible to simplify the Mueller calculus compared to linear polarization in order to recover index of refraction.
- Circularly polarized spherical illumination results in a much greater variation in the resulting Stokes reflectance field compared to linearly polarized spherical illumination. Hence, circular polarization has a better SNR for estimating specular roughness for dielectrics and metal composites, especially in conjunction with the proposed inverse rendering approach.

8 Conclusion and Future Work

In this paper we introduced a novel analysis of circularly polarized spherical illumination based on Mueller calculus, and presented a practical method to recover a more complete set of per-surface-point reflectance properties of objects based on this analysis. We demonstrated the technique with renderings under both environmental illumination and point lighting conditions that agree well with real photographs of the objects. We believe that the presented analysis of the Stokes reflectance field and its relation to material reflectance parameters is not only novel in the computer graphics and vision literature, but may also have application in applied optics. Contrary to traditional reflectance modeling that typically relies on observations of a material's response to several different lighting conditions, our method relies on observations under a *single* lighting condition. Hence, we believe this technique can also have applications in appearance modeling of large scale scenes with limited control over the incident illumination.

We also present the first practical technique in computer graphics to measure spatially varying index of refraction across an object's surface. This enables us to achieve more accurate results for SVBRDFs. Besides surface reflection, index of refraction plays a significant role in transmission in translucent media and in future work it would be interesting to apply such a measurement technique towards estimation of layered subsurface scattering. In this work, we also restrict ourselves to only circularly polarized incident illumination. In the future it would also be of interest to add a set of linearly polarized lighting conditions to estimate properties relating to the full Mueller matrix of how each surface point transforms incident polarized light to radiant polarized light. We believe such measurements would reveal additional properties of the material. Additionally, we would like to extend the index of refraction measurements to accurately capture the complex index of refraction of metallic materials.

Acknowledgments

We would like to thank Kaori Kikuchi for sitting as subject and Jay Busch for assistance in data processing. We are also grateful to Saskia Mordijck, Monica Nichelson, David Price, Bill Swartout, Randy Hill, and Randolph Hall for their support and assistance with this work. We also thank our anonymous reviewers for their helpful suggestions and comments. This work was sponsored in part by NSF grant IIS-1016703, the University of Southern California Office of the Provost and the U.S. Army Research, Development, and Engineering Command (RDECOM). The content of the information does not necessarily reflect the position or the policy of the US Government, and no official endorsement should be inferred.

References

ASHIKHMIN, M., PREMOZE, S., AND SHIRLEY, P. S. 2000. A microfacet-based BRDF generator. In *Proceedings of ACM SIGGRAPH 2000*, 65–74.

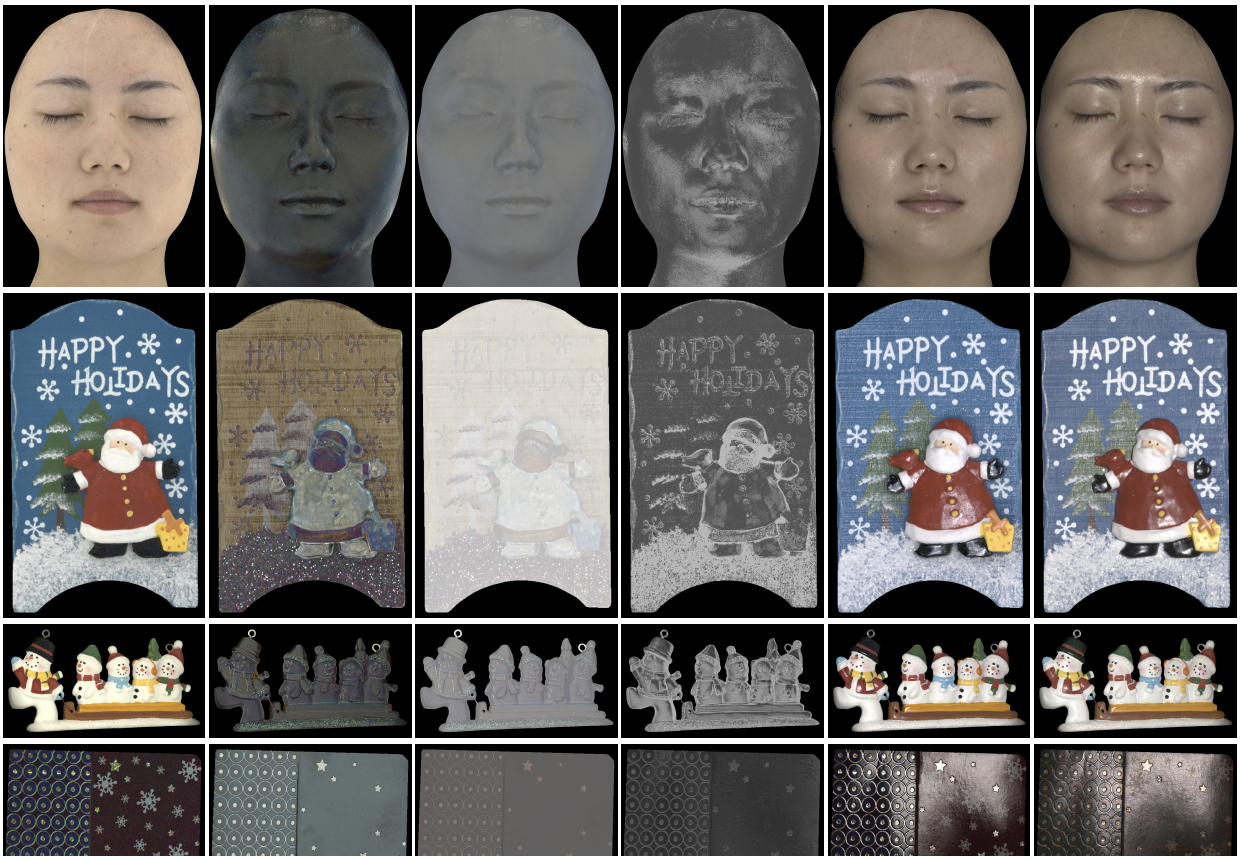

(a) diffuse albedo (b) specular albedo (c) index of refraction (d) specular roughness (e) rendering (f) photograph

Figure 11: ***Results:*** *Surface reflectance properties (**(a)-(d)**) estimated using circularly polarized spherical illumination. The estimated index of refraction **(c)** and specular roughness map **(d)** are used as the per pixel parameters for a Torrance-Sparrow BRDF to create renderings **(e)** that closely match the validation photographs **(f)** with illumination from the front.* ***Top-row****: a female subject.* ***Second-row****: a wooden wall hanging.* ***Third row****: specular christmas tree ornament.* ***Bottom-row****: a flat spatially varying BRDF sample.*

ATKINSON, G. A., AND HANCOCK, E. R. 2005. Multi-view surface reconstruction using polarization. In *ICCV*, 309–316.

ATKINSON, G. A., AND HANCOCK, E. R. 2007. Shape estimation using polarization and shading from two views. *PAMI 29*, 11, 2001–2017.

ATKINSON, G. A., AND HANCOCK, E. R. 2008. Two-dimensional brdf estimation from polarisation. *Comput. Vis. Image Underst. 111*, 2, 126–141.

CHEN, H., AND WOLFF, L. B. 1998. Polarization phase-based method for material classification in computer vision. *IJCV 28*, 1, 73–83.

COLLETT, E. 2005. *Field Guide to Polarization, SPIE Field Guides vol. FG05*. SPIE.

CULA, O. G., DANA, K. J., PAI, D. K., AND WANG, D. 2007. Polarization multiplexing and demultiplexing for appearance-based modeling. *PAMI 29*, 2, 362–367.

DANA, K. J., LIVESCU, G., AND MAKONAHALLI, R. 2009. Transparent watermarking using bidirectional imaging. In *IEEE International Workshop on Projector Camera Systems, in conjunction with CVPR*.

DEBEVEC, P., HAWKINS, T., TCHOU, C., DUIKER, H.-P., SAROKIN, W., AND SAGAR, M. 2000. Acquiring the reflectance field of a human face. In *ACM SIGGRAPH*.

GARDNER, A., TCHOU, C., HAWKINS, T., AND DEBEVEC, P. 2003. Linear light source reflectometry. In *ACM TOG*, 749–758.

GEORGHIADES, A. 2003. Recovering 3-D shape and reflectance from a small number of photographs. In *Rendering Techniques*, 230–240.

GHOSH, A., CHEN, T., PEERS, P., WILSON, C. A., AND DEBEVEC, P. E. 2009. Estimating specular roughness and anisotropy from second order spherical gradient illumination. *Comput. Graph. Forum 28*, 4, 1161–1170.

GOLDMAN, D. B., CURLESS, B., HERTZMANN, A., AND SEITZ, S. M. 2005. Shape and spatially-varying brdfs from photometric stereo. In *ICCV*, 341–348.

HE, X. D., TORRANCE, K. E., SILLION, F. X., AND GREENBERG, D. P. 1991. A comprehensive physical model for light reflection. *SIGGRAPH Comput. Graph. 25*, 4, 175–186.

HEALEY, G. 1992. Using color for geometry-insensitive segmentation. 52–69.

KOSHIKAWA, K. 1992. A polarimetric approach to shape understanding of glossy objects. 190–192.

LAFORTUNE, E. P. F., FOO, S.-C., TORRANCE, K. E., AND GREENBERG, D. P. 1997. Non-linear approximation of reflectance functions. In *SIGGRAPH '97*, 117–126.

LEE, S., KOO, H., CHO, N., AND PARK, J. 2006. Stochastic approach to separate diffuse and specular reflections. In *ICIP*.

LENSCH, H. P. A., GOESELE, M., KAUTZ, J., HEIDRICH, W., AND SEIDEL, H.-P. 2001. Image-based reconstruction of spatially varying materials. In *Rendering Techniques*, 103–114.

LENSCH, H. P. A., KAUTZ, J., GOESELE, M., HEIDRICH, W., AND SEIDEL, H.-P. 2003. Image-based reconstruction of spatial appearance and geometric detail. *ACM TOG 22*, 2, 234–257.

MA, W.-C., HAWKINS, T., PEERS, P., CHABERT, C.-F., WEISS, M., AND DEBEVEC, P. 2007. Rapid acquisition of specular and diffuse normal maps from polarized spherical gradient illumination. In *Rendering Techniques*, 183–194.

MALLICK, S. P., ZICKLER, T., BELHUMEUR, P. N., AND KRIEGMAN, D. J. 2006. Specularity removal in images and videos: A pde approach. In *ECCV*.

MARSCHNER, S. R., WESTIN, S. H., LAFORTUNE, E. P. F., TORRANCE, K. E., AND GREENBERG, D. P. 1999. Image-based BRDF measurement including human skin. In *Rendering Techniques*.

MATUSIK, W., PFISTER, H., BRAND, M., AND MCMILLAN, L. 2003. A data-driven reflectance model. In *ACM TOG*, 759–769.

MIYAZAKI, D., AND IKEUCHI, K. 2007. Shape estimation of transparent objects by using inverse polarization ray tracing. *PAMI 29*, 11, 2018–2030.

MIYAZAKI, D., KAGESAWA, M., AND IKEUCHI, K. 2003. Polarization-based transparent surface modeling from two views. In *ICCV*, 1381.

MIYAZAKI, D., KAGESAWA, M., AND IKEUCHI, K. 2004. Transparent surface modeling from a pair of polarization images. *PAMI 26*, 1, 73–82.

MÜLLER, V. 1996. Elimination of specular surface-reflectance using polarized and unpolarized light. In *ECCV*.

NAYAR, S., IKEUCHI, K., AND KANADE, T. 1990. Determining shape and reflectance of hybrid surfaces by photometric sampling. *IEEE Transactions on Robotics and Automation 6*, 4, 418–431.

NAYAR, S., FANG, X., AND BOULT, T. 1993. Removal of Specularities using Color and Polarization. In *CVPR*.

NAYAR, S. K., FANG, X.-S., AND BOULT, T. 1997. Separation of reflection components using color and polarization. *IJCV 21*, 3.

NICODEMUS, F. E., RICHMOND, J. C., HSIA, J. J., GINSBERG, I. W., AND LIMPERIS, T. 1977. Geometric considerations and nomenclature for reflectance. *National Bureau of Standards Monograph 160*.

PEERS, P., HAWKINS, T., AND DEBEVEC, P. 2006. A reflective light stage. Tech. Rep. ICT Technical Report ICT-TR-04.2006, ICT-USC.

PRIEST, R. G., AND GERMER, T. A. 2000. Polarimetric brdf in the microfacet model: theory and measurements. In *Proc. of the 2000 Meeting of the Military Sensing Symposia Specialty Group on Passive Sensors 1*, 169–181.

RAHMANN, S., AND CANTERAKIS, N. 2001. Reconstruction of specular surfaces using polarization imaging. *CVRP 1*, 149.

SADJADIZ, F., AND SADJADI, F. 2007. Extraction of surface normal and index of refraction using a pair of passive infrared polarimetric sensors. In *IEEE Conference on Computer Vision and Pattern Recognition*, 1–5.

SAITO, M., SATO, Y., IKEUCHI, K., AND KASHIWAGI, H. 1999. Measurement of surface orientations of transparent objects by use of polarization in highlight. *J. Opt. Soc. Am. A 16*, 9, 2286–2293.

SHAFER, S. 1985. Using color to separate reflection components. *COLOR Research and Applications 10*, 4.

THILAK, V., VOELZ, D. G., AND CREUSERE, C. D. 2007. Polarization-based index of refraction and reflection angle estimation for remote sensing applications. *Appl. Opt. 46*, 30, 7527–7536.

TOMINAGA, S., AND YAMAMOTO, T. 2008. Metal-dielectric object classification by polarization degree map. In *CVPR*, 1–4.

TORRANCE, K. E., AND SPARROW, E. M. 1967. Theory of off-specular reflection from roughened surfaces. *J. Opt. Soc. Am. 57*, 1104–1114.

UMEYAMA, S., AND GODIN, G. 2004. Separation of diffuse and specular components of surface reflection by use of polarization and statistical analysis of images. *PAMI 26*, 5.

WARD, G. J. 1992. Measuring and modeling anisotropic reflection. *SIGGRAPH Comput. Graph. 26*, 2, 265–272.

WOLFF, L. B., AND BOULT, T. E. 1991. Constraining object features using a polarization reflectance model. *PAMI 13*, 7, 635–657.

WOLFF, L. B. 1989. Surface orientation from two camera stereo with polarizers. In *Proc. SPIE Conf. Optics, Illumination and Image Sensing for Machine Vision IV*, vol. 1194, 287–297.

WOLFF, L. B. 1990. Polarization-based material classification from specular reflection. *PAMI 12*, 11, 1059–1071.

ZICKLER, T., RAMAMOORTHI, R., ENRIQUE, S., AND BELHUMEUR, P. N. 2006. Reflectance sharing: Predicting appearance from a sparse set of images of a known shape. *PAMI 28*, 8, 1287–1302.